

## Thin Films

## Efficient Sensing of Explosives by Using Fluorescent Nonporous Films of Oligophenyleneethynylene Derivatives Thanks to Optimal Structure Orientation and Exciton Migration

Thomas Caron,<sup>[a]</sup> Eric Pasquinet,<sup>[a]</sup> Arie van der Lee,<sup>[b]</sup> Robert B. Pansu,<sup>[c]</sup> Vincent Rouessac,<sup>[b]</sup> Simon Clavaguera,<sup>[a]</sup> Myriam Bouhadid,<sup>[a]</sup> Françoise Serein-Spirau,<sup>[d]</sup> Jean-Pierre Lère-Porte,<sup>[d]</sup> and Pierre Montméat<sup>\*[a]</sup>

**Abstract:** The fluorescence of thin films of a diimine-substituted phenyleneethynylene compound can be efficiently quenched by nitroaromatic vapors, which is not the case for the unsubstituted parent compound. Thin-film porosity is usually considered to be an essential factor for efficient quenching, but in the present case the origin of the quenching is completely different, as both films are nonporous and hermetic to 2,4-dinitrotoluene (DNT) molecules. The molecular organization in the two crystallized thin films offers a low level of  $\pi$  stacking for both compounds, but the orientation of the phenyleneethynylene fluorophore differs markedly

with respect to the surface of the films. For the substituted compound, the fluorophore is almost parallel to the surface, thus making it readily available to molecules of a nitroaromatic quencher. This rationale is also observed in the case of a related compound bearing methoxy side chains instead of the long octyloxy moieties. Fluorescence-lifetime experiments show that the efficient quenching process in the nonporous crystallized films of the substituted compound is due to a fast (<70 ps) diffusion of excitons from the bulk of the film toward the surface where they are quenched, thus providing evidence of antenna effects.

## Introduction

The reliable and sensitive detection of hidden explosives in luggage, cars, or aircraft is currently a major issue for law-enforcement agencies that face the continuous threat of sudden terrorist attacks. The detection of millions of landmines that have remained unexploded in civil areas during several military conflicts is another concern for military demining sections. Various technologies for the detection of explosives, including HPLC, Electron capture detector, GC-MS, X-ray imaging, and ion-mobility, IR, and NMR spectroscopy,<sup>[1]</sup> have been developed

over the years, but the cost, portability, and complexity of many of these methods are unsuitable for monitoring devices on site.

For this reason, recent research has focused on the development of portable, low-cost, and reliable detection devices. A suitable sensor is also required to analyze samples in a relatively short time. In the particular case of landmine detection, a system that avoids physical contact with the target is needed.<sup>[2]</sup> A variety of chemical sensors have been developed based on various transductions. Mass sensors have well-suited detection properties,<sup>[3]</sup> but in most cases they fail to detect explosives with very low vapors pressures. Optical devices based on immunosensors exhibit high selectivities thanks to the specific reaction of antibodies with explosives molecules.<sup>[4]</sup>

Despite these advances, there is still a strong demand for explosive-vapors sensors to be utilized for the inspection of suspicious luggage, forensic analysis, and landmine detection. As trinitrotoluene (TNT) is one of the most commonly used explosives for military applications, it represents a significant target when carrying out detection for bombs hidden in battle fields or luggage, thus stimulating a growing amount of research over recent years.<sup>[5]</sup> This is also true for 2,4-dinitrotoluene (DNT), a residual product of TNT synthesis that has a significant part in the chemical signature of TNT,<sup>[6]</sup> because the vapor pressure of DNT is two orders of magnitude higher than TNT (i.e., 148 versus 6 ppbv at 20 °C; ppbv = parts per million by volume).<sup>[7]</sup>

[a] Dr. T. Caron, Dr. E. Pasquinet, Dr. S. Clavaguera, Dr. M. Bouhadid, Dr. P. Montméat  
CEA-DAM Le Ripault, BP 16, 37260 Monts (France)  
Fax: (+33)247345142  
E-mail: pierre.montmeat@cea.fr

[b] Dr. A. van der Lee, Dr. V. Rouessac  
Institut Européen des Membranes, ENSCM-UM2-CNRS UMR5635  
cc047 Université Montpellier, 2 Place Eugène Bataillon  
34095 Montpellier (France)

[c] Dr. R. B. Pansu  
ENS Cachan, CNRS, UMR8531 and IFR d'Alembert IFR 3242  
61, Avenue du Président Wilson, 94235 Cachan (France)

[d] Prof. F. Serein-Spirau, Prof. J.-P. Lère-Porte  
Institut Charles Gerhardt, UMR CNRS 5253, Equipe AM2N  
Ecole Nationale Supérieure de Chimie de Montpellier  
8, Rue de l'École Normale, 34296 Montpellier (France)

Supporting information for this article is available on the WWW under <http://dx.doi.org/10.1002/chem.201402271>.

Previous studies have demonstrated the potential of optical sensors for the detection of DNT,<sup>[8]</sup> and especially  $\pi$ -conjugated polymers have attracted a great deal of attention as nitroaromatic sensing materials.<sup>[9]</sup> In particular, a number of polyphenylenevinylene and polyphenyleneethynylene polymers have been shown to undergo fluorescent extinction upon exposure to nitroaromatic vapors. Generally speaking, the efficiency of these sensing materials is mostly attributed to an amplification effect based on conjugation and to the presence of cavities in the film.<sup>[9a–g]</sup> Polymer **1** is a typical example in this field. Therefore, other structures have been designed to create sensitive films with minimal  $\pi$  stacking and maximum porosity to enable a certain degree of permeability to nitroaromatic vapors.<sup>[10]</sup> To achieve this goal, we have previously reported the development of an alternate  $\pi$ -conjugated polymer **2** based on a 1,2-diiminocyclohexane chiral unit that exhibits fluorescent quenching in the presence of DNT vapors.<sup>[11]</sup> However, we have also demonstrated the high sensing ability of the related monomeric diimine **3a** toward both DNT and TNT vapors<sup>[12]</sup> (Scheme 1). Moreover, a few other nonpolymeric compounds have recently been described for the same purpose.<sup>[13]</sup>

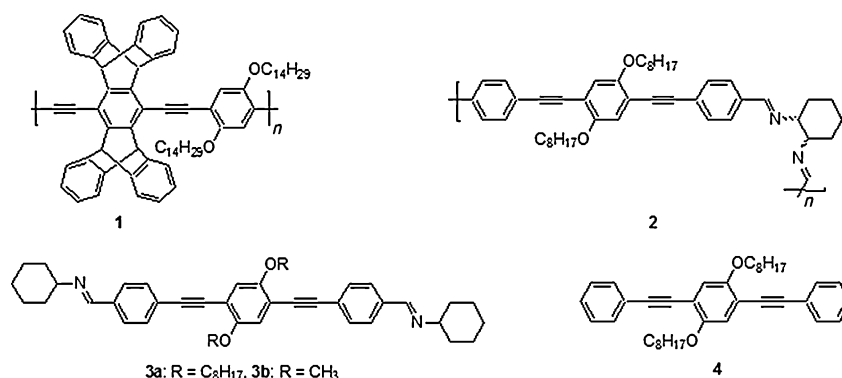
Nevertheless, there is no rationale that explains how these compounds can efficiently detect nitroaromatic vapors. In this light, we report herein on the three-dimensional molecular arrangement within the crystals that constitute the films of **3a** and of a similar compound that is much less sensitive to nitroaromatic vapors. We show how the different molecular packing in the films of these two compounds can account for their markedly different sensing efficiencies. Time-resolved fluorescence experiments also provide evidence of an amplification phenomenon through exciton migration to account for the high sensitivity of films of **3a** despite a lack of porosity.

## Results and Discussion

### Nitroaromatic sensing

Thin films (thickness  $\approx$  30 nm) of diimine-functionalized phenyleneethynylene **3a** and the related compound **4** (Scheme 1) were exposed to DNT vapors (Figure 1).

Although the fluorescence extinction of the films of **3a** reached 51%, the films of **4** exhibited only a very weak response (10%). The observed higher sensitivity of **3a** toward DNT can be first understood in terms of HOMO and LUMO energetic levels. According to cyclic-voltammetric measurements, the HOMO level of both compounds was  $-5.68$  eV, whereas the LUMO levels of **3a** and **4** were  $-2.57$  and  $-2.52$  eV, respectively. Moreover, the optical-band gaps of **3a** and **4** are 2.94 and 3.10 eV, respectively. These energetic levels demonstrate



**Scheme 1.** Known polymers for the detection of nitroaromatic explosives and related nonporous compounds studied in this work.

that **4** should be more prone to quenching in solution through photoinduced electron transfer by a DNT molecule than **3a**. In addition, the Stern–Volmer quenching constant ( $K_{SV}$ ), determined in THF as the slope of the relative fluorescence intensity plotted as a function of the DNT concentration, was lower for **3a** than for **4** (79 vs. 119 L mol<sup>-1</sup>, respectively).<sup>[11b]</sup> This first set of results prompted us to carry out further characterization to understand the significantly higher sensor efficiency of **3a** relative to **4** in the solid state.

BET surface areas ( $SA_{BET}$ ) were very low for powders of **3a** (i.e., 2.9 m<sup>2</sup>g<sup>-1</sup>). However, these  $SA_{BET}$  values were obtained for powders at 77 K, and the results could not be extrapolated directly to a case of thin-deposited films, that is, with more flexible material networks when the ad/absorption is carried out at room temperature and with a small macroscopic-access area relative to the powders. A specific setup was used to investigate the adsorption properties of **3a**. This setup can be considered to be a BET adsorption equipment, but for which the measurements are directly carried out on thin films; therefore, the mass-uptake isotherm of the film due to vapor ad/absorption is acquired by means of a quartz-crystal microbalance (QCM). The adsorption curves of polypentiptycene **1** developed by Yang and Swager,<sup>[9d]</sup> diimine **3a**, related polymer **2**,<sup>[11]</sup> and model compound **4** in toluene<sup>[14]</sup> are presented in Figure 2.

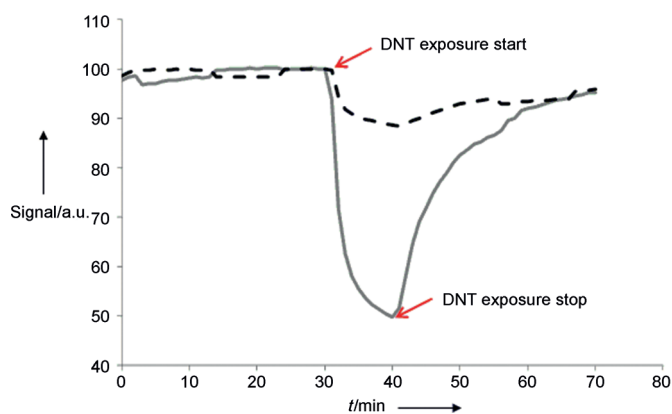


**Figure 1.** Fluorescence quenching of **3a** and **4** upon exposure to DNT (bold line: **3a**, dotted line: **4**).

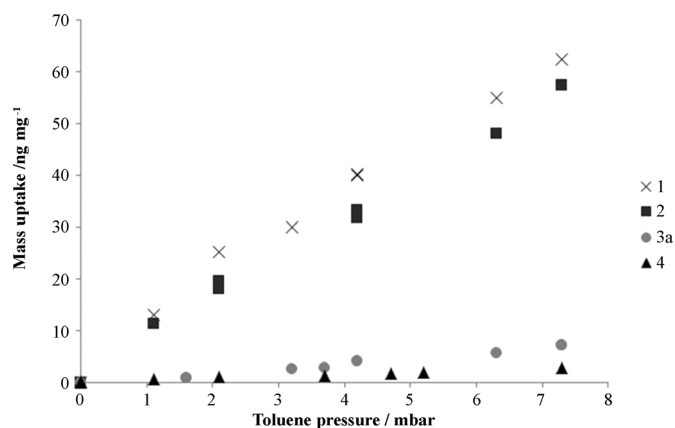


**Figure 2.** Toluene ad/absorption efficiency in thin films of compounds **1**, **2**, **3a**, and **4**.

Although the films of specifically designed polymers, such as poly(penttiptycene **1** and polyimine **2**, seem to readily adsorb toluene vapors, the profile of **3a** shows a low mass uptake, which corresponds to a type-II or -III isotherm<sup>[15]</sup> that is commonly obtained for either nonporous or macroporous materials. This proposition was confirmed by testing the powders, thus classifying **3a** as nonporous. Interestingly, similar results (a very low  $S_{\text{A}_{\text{BET}}}$  value of  $0.4 \text{ m}^2\text{g}^{-1}$  and nearly flat sorption isotherm) were obtained for **4**, which is structurally related to **3a**, but is almost completely insensitive to nitroaromatic vapors. Therefore, the hypothesis of markedly dissimilar porosities to explain the different sensing abilities has to be ruled out when considering the nonporous, poorly sensitive **4** and the nonporous, highly sensitive **3a**. This outcome is noteworthy because the efficiency of a number of related  $\pi$ -conjugated oligomers or polymers has been attributed to their porosity in the solid state, even though the  $S_{\text{A}_{\text{BET}}}$  values were almost never given. We measured the  $S_{\text{A}_{\text{BET}}}$  value of poly(penttiptycene **1** developed by Yang and Swager to be  $36 \text{ m}^2\text{g}^{-1}$ ,<sup>[12a]</sup> which proves that this material is truly porous, in sharp contrast with **3a** and **4**. Therefore, the detection mechanisms are clearly different in these latter cases, and surface phenomena, rather than bulk events, should be invoked.

Both **3a** and **4** result in heterogeneous films when deposited on glass substrates. SEM micrographs of these spin-coated thin films are provided in the Supporting Information. It appeared that the coated surfaces were constituted of flakelike particles (up to  $1 \mu\text{m}$  in length, some of which can be seen as darker objects in the micrograph of **3a**). These objects were assumed to be crystallites.

### XRD studies

The presence of crystallites as observed in the SEM micrographs prompted us to investigate the crystal structure of the films. X-ray diffractograms were recorded on spin-coated films, and similar patterns were obtained for both **3a** and **4** (see the Supporting Information); that is, a single strong Bragg peak at low angles was observed, which is indicative of a high degree of crystallization and a strongly preferred orientation. Suitable

single crystals for a full structural X-ray characterization were grown and analyzed to elucidate the molecular structure and packing. The first strong low-angle peak calculated from the structural data obtained by using the single crystals corresponded exactly with those peaks observed in the diffractograms of the films. This result made us confident that all the information taken from the single-crystal structure determination could be extrapolated to the molecular structure of the films. Complete crystallographic data and structure models embedded as a manipulable three-dimensional content are given in the Supporting Information.

The first point was that crystals of **4** were of higher density and compacity than those of **3a**, without any free volume inside. Conversely, crystal packing of **3a** revealed channels (see the Supporting Information) and a free volume of 1.2%. As such, **3a** can, according to the definition by Holst et al.,<sup>[16]</sup> be considered as an extrinsically porous molecule, and we first believed that these different properties could account for the better detection of nitroaromatic compounds exhibited by the films of **3a**. However, the sizes of these channels were much too small (mean radius =  $1 \text{ \AA}$ ) to accommodate DNT or TNT molecules. This finding was further demonstrated by recording a diffractogram of **3a** crystals in the presence of DNT vapors (exposure time = 7 days; see the Experimental Section for a description of the setup), and a diagram was acquired that was identical to the image obtained without DNT vapors, thus indicating that DNT molecules do not penetrate the crystals at a loading fraction that could explain 51% quenching of the fluorescence. Therefore, **3a** should definitely be considered as hermetic toward nitroaromatic vapors, and the efficiency of **3a** in the detection of these species cannot be attributed to any porosity of the films, contrary to related conjugated materials.

Compound **3a** crystallizes in the monoclinic system  $P2_1/c$  (Figure 3). The asymmetric unit of **3a** shows that the three aromatic rings are almost planar (angle between the external and central rings =  $6^\circ$ ) as are the imine functions. This finding is consistent with the expected high delocalization of the  $\pi$  electrons. On the other hand, the cyclohexyl rings are tilted from the plane (angle =  $74.5^\circ$ ), thus indicating steric hindrance. The most remarkable feature, however, is the near perpendicularity of the two octyloxy side chains at C3 (angle measured between C1 and C5 =  $87^\circ$ ). This angle is unexpected because such alkoxy chains are often linear, as reported for related phenyleneethynylene structures.<sup>[17]</sup> In the mesh structure, the top and bottom faces both comprise five molecules that form an S shape due to the presence of one tilted molecule that bridges over two parallel pairs. The aromatic nuclei in each of these pairs are not plane-to-plane stacked. Indeed, a J-type aggregation<sup>[18]</sup> that we believe to be induced by the cyclohexyl moieties seems to avoid any  $\pi$  stacking. This finding is consistent with the high solid-state quantum yield recorded for the films (41%).

A projection along the  $b$  axis clearly shows a lamellar organization along the  $a$  axis. The crystal plane (1,0,0) is parallel to the surface and the  $\pi$ -conjugated structure is slightly tilted ( $21^\circ$ ) from this plane. The gap between each leaflet is filled with the octyloxy chains that interact with each other thanks

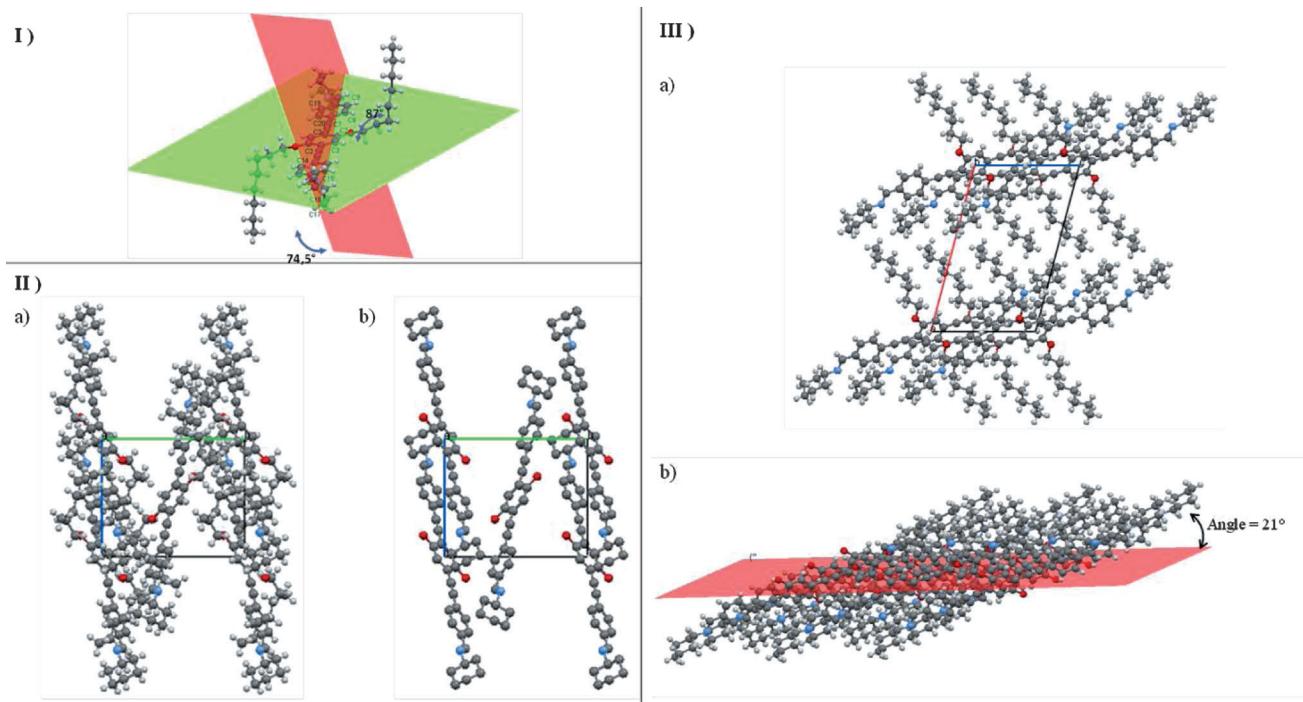


**Figure 3.** Crystallographic investigation of **3a**. I) The asymmetric unit and planes formed by the aromatic nuclei (in green) and cyclohexyl function (in red). II) Projection of the mesh according to the  $a$  axis: a) complete mesh, b) simplified mesh (side chains are omitted for the sake of clarity). III) Projection of the mesh according to the  $b$  axis: a) complete mesh, b) lamellar organization along the  $a$  axis (side chains are omitted for the sake of clarity).

to van der Waals forces, which presumably accounts for the unusual bend conformation of these side chains.

Compound **4**, which also crystallizes in space group  $P2_1/c$ , is represented in Figure 4. In the asymmetric unit, the three aromatic rings are not fully coplanar, with angles of 12.3 and 20.9° between the central ring and each of the external counterparts. In sharp contrast with **3a**, all the carbon atoms in the side chain are coplanar and adopt an angle of 60° with the mean plane formed by the aromatic nuclei. The mesh comprises four molecules that form two crosses, as evidenced upon projection along the  $a$  axis (Figure 4). This structure obviously renders possible low-level  $\pi$  stacking, which results in a reasonably high solid-state quantum yield for the films (33%). A la-

mellar organization appears along the  $c$  axis, with leaflets that consist of a series of crosses. Only harmonic peaks ( $h00$ ;  $h = 1,2,3$ ) are observed in the diffractogram measured under symmetric Bragg–Brentano conditions, thus the only crystal plane that is parallel to the film must be the (100) plane. The  $\pi$ -conjugated structure is highly tilted (60°) from this plane and, thus, from the film surface.

The XRD study highlights a number of similarities in the thin crystallized films of **3a** and **4**, that is, a lack of porosity, low  $\pi$ -stacking, and a lamellar organization parallel to the substrate surface. But the markedly different angles between the lamellar planes parallel to the substrate surface and the  $\pi$ -conjugated system led us to the following hypothesis: the quenching

by nitroaromatic compounds, such as DNT or TNT, involves an electron transfer<sup>[19]</sup> that requires an orbital overlap between the quencher and the  $\pi$ -conjugated system. Therefore, for an efficient detection, the  $\pi$  system of the fluorescent probe has to be appropriately oriented to make the nitroaromatic quencher approach and interaction efficient. The small angle in **3a** enables such an approach and the quenching is high. Due to a large angle in the case of **4**, only the sides of the aromatic compounds are exposed to the

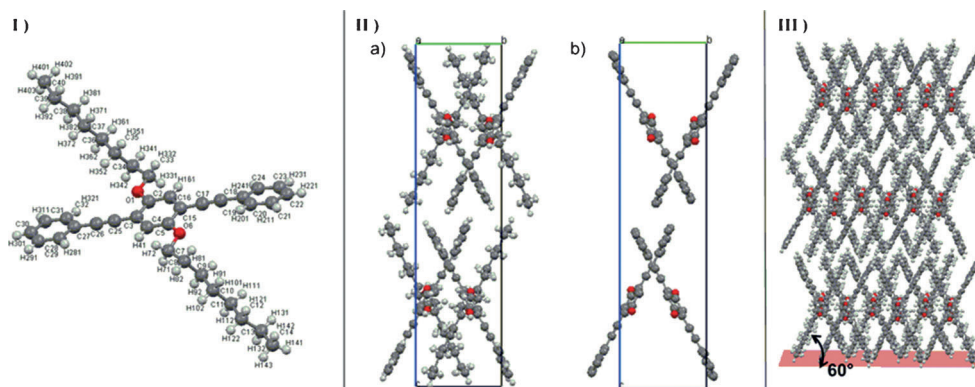


**Figure 4.** Crystallographic investigation of **4**. I) Asymmetric unit. II) Projection of the mesh according to the  $a$  axis: a) complete mesh, b) simplified mesh (side chains are omitted for the sake of clarity). III) Lamellar organization along the  $c$  axis.

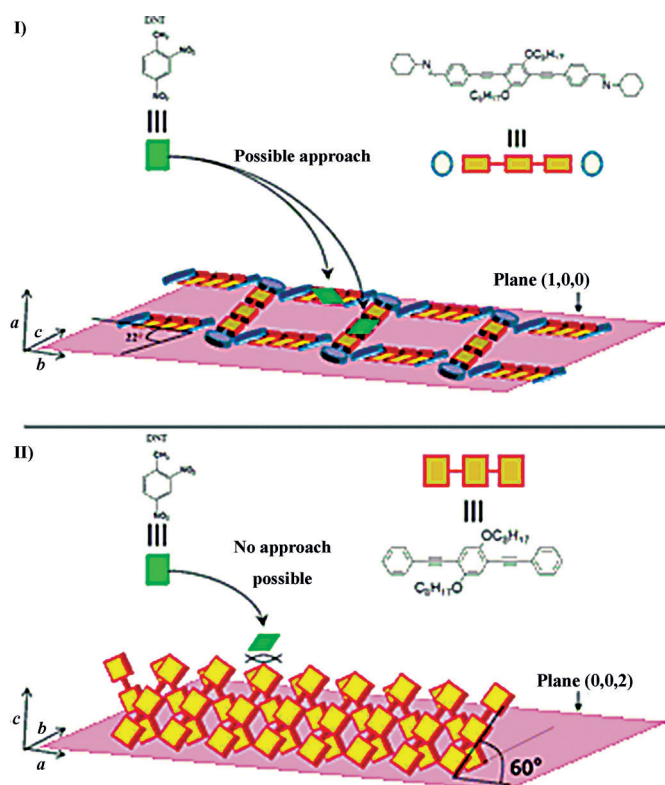


**Figure 5.** Schematic view of the interaction between the nitroaromatic quencher and the  $\pi$ -conjugated system at the surface of films of **3a** (I) and **4** (II).

nitroaromatic quencher, thus accounting for the poor detection ability of films of **4** relative to the **3a** counterparts. This process is schematically represented in Figure 5.

This hypothesis was further validated by studying **3b**, an analogous diimine derivative bearing short methoxy substituents. Although the octyloxy chains, which have been shown to play a significant role in the supramolecular organization of films of **3a**, are absent in the case of **3b**, a lamellar organization with a small angle of 22.5° between the substrate and the  $\pi$ -conjugated system can also be observed for films of **3b**. This outcome correlates well with a high fluorescence quenching value (60%) in the presence of DNT vapors (see the Supporting Information).

These results clearly show that nonporous oligomers such as **3a,b** can represent a promising alternative to porous conjugated materials for the detection of nitroaromatic vapors. Here, the texturation and orientation in the solid state seem to drive the gas-detection performance and outweigh other effects. For example, chemical affinity or electronic effects are not the major contributors in the solid-/gas-detection process. As a matter of fact,  $K_{SV}$  values and HOMO–LUMO levels, determined in solution, indicate that **3a** is intrinsically less efficient as a sensitive material than **4** (see the section on nitroaromatic sensing), whereas this outcome is not what we observed for solid films.

### Antenna effects in films of **3a**

Considering the film thicknesses (ca. 30 nm) and the mesh heights (17.7 and 14.2 Å for **3a** and **3b**, respectively) only a small fraction of **3a** and **3b** molecules are present at the surface of the film (close to 20%) and are supposed to interact with the gas. Therefore, due to their lack of porosity, significant quenching values (> 50%) can only be achieved if some kind of amplification phenomenon takes place. One hypothesis is that exciton migration occurs within the crystallized films and creates an antenna effect.<sup>[19g,20]</sup>

This proposition prompted us to investigate the properties of thin films of **3a** by using time-resolved fluorescence. Indeed, the diffusion of the excitation to the surface is in the nanosecond range, whereas the diffusion of the DNT molecules inside the film would be much slower. In the absence of DNT vapors, the excited molecules of **3a** last for a few nanoseconds before they emit a photon. In the presence of DNT, the molecules at the surface transfer an electron to the DNT in a few picoseconds with no emission of the photon;<sup>[21]</sup> in other words, they become quenched. For the molecules deeper in the bulk of the film, the excitation (exciton) first hops from molecule to molecule through dipolar coupling (such as fluorescence resonance energy transfer (FRET)) until the exciton reaches a DNT molecule where it is quenched. Thus, in the presence of DNT, the time during which excitons can emit photons depends on their initial position in the film. Decay of the fluorescence intensity after a short laser pulse follows multiexponential kinetics, which is well described by the laws of diffusion.<sup>[22]</sup>

The decay of the fluorescence of thin films of **3a** after a pulse excitation (1 ps) was recorded during exposure to DNT vapors. The intensity of the fluorescence drops by 55% upon exposure of the film (Figure 6a), which correlates well with the quenching measured with the prototype system (Figure 1; thickness  $\approx$  30 nm). The drop in fluorescence intensity takes 45 seconds and the recovery lasts for 60 seconds. We attribute these values to the mixing time in the exposure chamber. The intensity and fluorescence lifetime drop by 25%. The response time is the same as that of the intensity. This change in the fluorescence lifetime is confirmation of the presence of a dynamic quenching mechanism in addition to direct quenching by contact. If only the surface molecules that can exchange electrons with the adsorbed DNT molecules had become quenched, we would have seen a drop in fluorescence intensity without an accompanying change in the lifetime.

To obtain further information on that dynamic process, the shape of the fluorescence decays was recorded (Figure 6b). The decay in the absence of DNT is mostly exponential (85% of the initial fluorescence at 1 ns, 15% at 2.5 ns). When DNT is added, the decay becomes faster and particularly presents an initial sharp decay. The decay without the presence of a quencher represents the solution of the excited-state kinetics equation [see Eq. (E1) in the Supporting Information] without diffusion. Because the intramolecular deactivation rate does not depend on the position, the contribution of the quenching by diffusion of the exciton to the decay can be obtained by di-

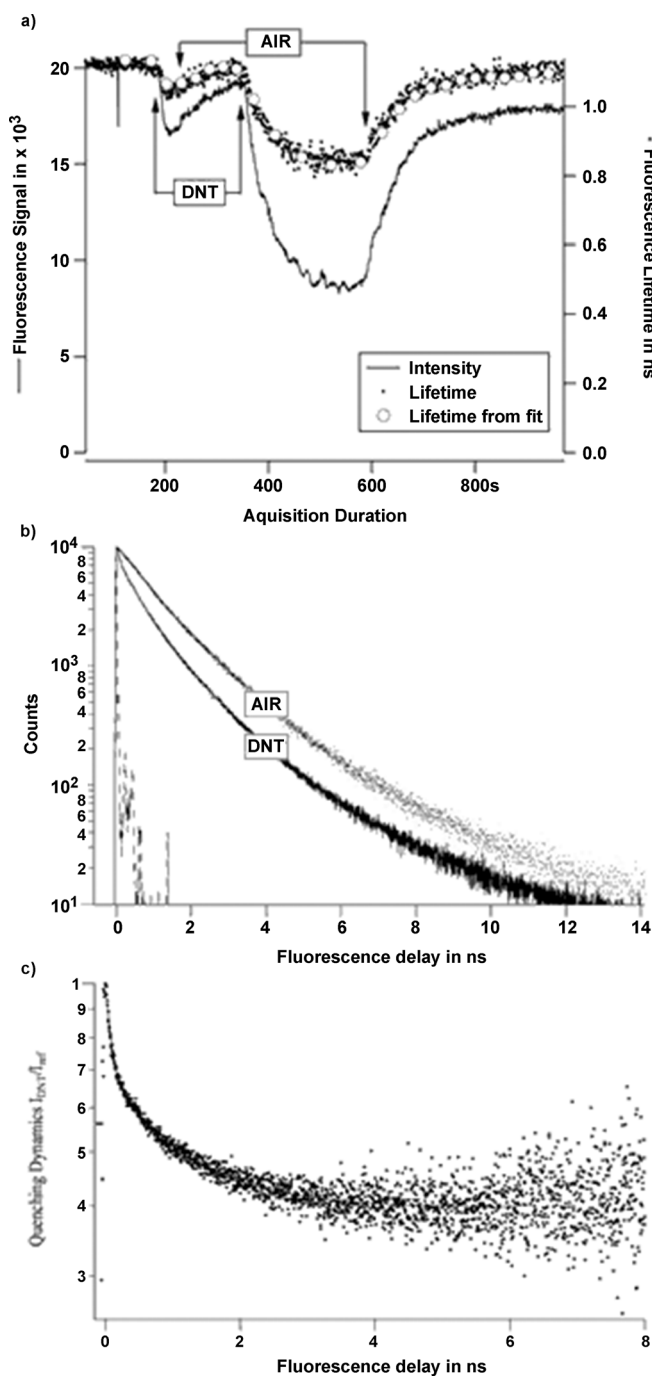


**Figure 6.** Time-resolved fluorescence characterization of **3a**. a) Intensity and fluorescence lifetime upon exposure of a film of **3a** ( $\lambda_{ex} = 345$  nm,  $\lambda_{em} > 400$  nm) to DNT vapors. Quenching of the intensity by more than 50% is observed and accompanied by a drop in fluorescence lifetime. The lifetime was estimated as the average of time between laser excitation and photon detection every second (dots) or by fitting the fluorescence decay curve every 30 seconds (open circles). b) Fluorescence decay without DNT ( $I_{ref}$ , dots) and with DNT ( $I_{DNT}$ , line). The decay of **3a** is mostly exponential. A fast component with a lifetime of 230 picoseconds appears in the presence of DNT due to the dynamic quenching. c)  $I_{DNT}/I_{ref}$ : the drop in the fluorescence lifetime is due to quenching of 60% of the dyes with a multiexponential signature and an initial decay time of less than 70 picoseconds. This process is characteristic of barrierless diffusion; that is, diffusion of the exciton toward the surface where it reacts with DNT.

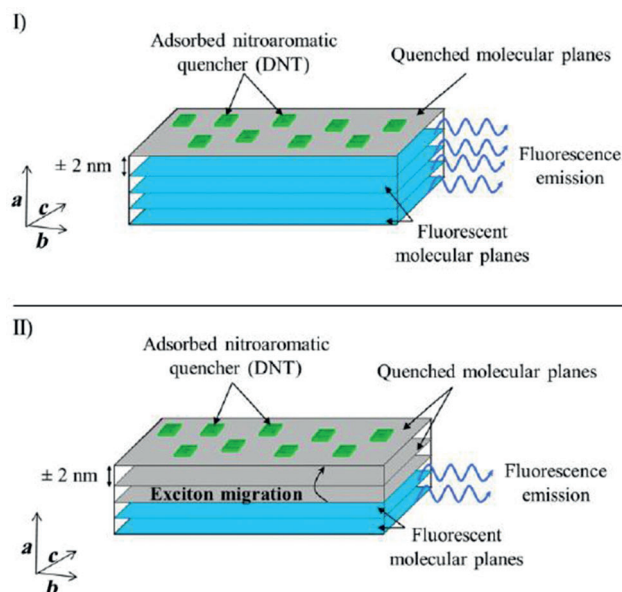


**Figure 7.** Schematic representation of antenna effects within the crystallized films of **3a**.

viding the decay obtained in the presence of the quencher by the corresponding value obtained in the absence of the quencher [see Figure 6c and Eq. (E3) in the Supporting Information]. It is apparent that the dynamics of the quenching are extremely fast ( $< 75$  ps) at time zero, which is characteristic of a barrierless diffusion process. This diffusion is much faster than that of DNT into the crystallized nonporous films of **3a** because this process was shown to take a fraction of a second for a soft polymer.<sup>[23]</sup> The process is also fast relative to the time it takes for DNT vapors to diffuse from the gas phase to the surface of the film – a diffusion that depends on the vapors pressure of DNT (i.e., 150 ppb)<sup>[7]</sup> and the speed of a perfect gas at room temperature.

The diffusion time can be estimated to be 60 nanoseconds. The fast reaction observed corresponds to the reaction with DNT molecules already adsorbed on the crystal surface. Figure 6 also reveals quenching levels at 60%. Half of the molecules are too deep inside the film for their fluorescence to be sensitive to the surface reaction. Thus, a change in the fluorescence lifetime is evidence that the quenching of the fluorescence is a dynamic process that cannot be ascribed to the diffusion of DNT molecules inside the films, but to the diffusion of the excitation in the crystal toward the surface where the DNT molecules are adsorbed (this process is schematically represented in Figure 7).

The quenching is mostly reversible (Figure 6a), but we note an irreversible drop of the fluorescence intensity by 10%. The quenching, as determined by using lifetime measurements, is fully reversible. The DNT molecules are successfully flushed away from the surface. The loss in intensity corresponds to the disappearance of fluorescent molecules during the detection process, which is 5000-fold larger than the bleaching measured for a sample not exposed to DNT. Thus, a specific photoreaction might occur in the presence of DNT, thus producing non-fluorescent nonquenching photoproducts.

## Conclusion

A crystallographic investigation and time-resolved fluorescence experiments have been carried out on thin films of phenyleneethynylene compounds, thus providing initial insight into their structure/sensing-ability relationships. Despite the lack of porosity of these films, the fluorescence of films of **3a** and **3b** is efficiently quenched thanks to migration of the excitons in the bulk toward the film surface where gaseous nitroaromatic molecules can readily access the  $\pi$ -conjugated structure that is almost parallel to the film surface.

## Experimental Section

### Synthesis

The synthesis of **4** has been described elsewhere.<sup>[24]</sup> Compounds **3a** and **3b** were obtained through the reaction of cyclohexylamine with the corresponding dialdehydes. The synthetic procedures and compound characterizations are provided in the Supporting Information.

### Film deposition and characterization

The materials were deposited on the entire surface of a glass substrate (Heathrow Scientific; microscope slides = 75 × 25 × 1 mm) by spin-coating (Braive Instrument; spin-coater = 600 rpm) from a solution in THF followed by 60 s of drying. SEM micrographs of spin-coated thin films of **3a** and **4** were obtained on a Hitachi S4500 microscope. The spectroscopic film properties, that is, absorption and emission, were determined on a PerkinElmer Lambda 35 and a Jobin-Yvon Fluoromax 3 instrument, respectively. The optical densities of the films were around 0.2 at  $\lambda = 374$  and 418 nm for **4** and **3a,b** (the absorption and emission spectra are given in the Supporting Information). The thickness of the film of **3a** was evaluated with a profilometer or atomic force microscopy (AFM). An absorbance of 0.2 led to a thickness of approximately 30 nm. Solid-state quantum yields were obtained on a Hamamatsu C9920-02 spectrometer.

### Detection tests

A laboratory-made prototype was used. The central element was a coated microscope slide that acted both as the transducer and substrate of the active material. A more detailed description of the instrument has been given elsewhere.<sup>[12b,25]</sup> Each fluorescent material was evaluated for the detection of DNT in dry synthetic air. A specific setup was used to generate DNT vapors and expose the film to 150 ppbv of DNT. The sensor response was expressed as the percentage of fluorescence quenched after 10 minutes.

### Determination of HOMO and LUMO levels

Electrochemical measurements were performed with a standard three-electrode system that consisted of a Pt working electrode, a Pt-wire counterelectrode, and an Ag/Ag<sup>+</sup> reference electrode in a solution of TBAPF<sub>6</sub> (0.1 M) in freshly distilled acetonitrile.

### Adsorption experiments

BET surface areas ( $SA_{\text{BET}}$ ) were evaluated for powders of **3a** and **4** (120 and 570 mg, respectively) under N<sub>2</sub> at 77 K on a Micromeritics TriStar 3000 tool. Adsorption characterization on deposited films

were carried out by using a laboratory-made setup that coupled vapor adsorption with quartz-crystal-microbalance gravimetry. The equipment could measure the small mass uptake of a deposited thin film on a dedicated quartz crystal due to gas ad/absorption.<sup>[26]</sup> The principal advantages of this coupled technique relative to the classic volumetric BET setup that used nitrogen or another gas at low temperature are 1) a high sensitivity that enabled the analysis of the ab/adsorption of deposited nanoporous thin films with thicknesses that ranged from 10 nm to approximately 100 nm; 2) the process was carried out at room temperature, thus rendering possible analysis of flexible materials; and 3) an ability to use several gases other than classical N<sub>2</sub> at 77 K, with a high vapor pressure (below 1 bar for our setup).<sup>[27]</sup>

### Crystallographic studies

The X-ray data collection of the single crystals was performed at 173 K on an Oxford-Diffraction GEMINI-S single-crystal diffractometer by using graphite-monochromatized MoK $\alpha$  radiation ( $\lambda = 0.71073$  Å). The 3D structures were solved by ab initio methods, such as those implemented in the charge-flipping algorithm.<sup>[28]</sup> The structural refinements were performed by using the CRYSTALS package<sup>[29]</sup> on  $F_{\text{obs}}$  with reflections at  $I > 2\sigma(I)$ . The data collection of the films was carried out with a PANalytical X'pert MPD powder diffractometer equipped with a X'celerator detector with CuK $\alpha$  radiation ( $\lambda = 1.5418$  Å). Experiments were also recorded in a DNT atmosphere. A special tight sample holder was used in which small amounts of DNT were placed close to the powder sample.

CCDC-881459–881461 contain the supplementary crystallographic data for this paper. These data can be obtained free of charge from The Cambridge Crystallographic Data Centre via [www.ccdc.cam.ac.uk/data\\_request/cif](http://www.ccdc.cam.ac.uk/data_request/cif).

### Time-resolved fluorescence experiments in the presence of DNT vapors

Solid DNT was equilibrated with air in an Erlenmeyer flask (120 mL), and the gas was sucked out with a syringe and sent to the exposition chamber under a microscope by means of plastic tubes. A diagram of the setup is given in the Supporting Information. The fluorescence lifetime setup<sup>[30]</sup> and the fluorescence lifetime imaging microscopy (FLIM) setup have been described elsewhere.<sup>[31]</sup>

## Acknowledgements

The authors wish to thank Vincent Frotté (CEA-DAM Le Ripault) for performing the BET analysis and Didier Cot (Institut Européen des Membranes) for the SEM pictures.

**Keywords:** photoluminescence · sensors · structure–property relationships · supramolecular materials · surfaces and interfaces · thin films

[1] D. S. Moore, *Sens. Imaging* **2007**, *8*, 9–38.

[2] M. La Grone, C. Cuming, M. Fisher, M. Fox, S. Jacob, D. Reust, M. Rockley, E. Towers, *Proc. SPIE-Int. Soc. Opt. Eng.* **2000**, *4038*, 553–562.

[3] a) P. Montméat, S. Madonia, E. Pasquinet, L. Hairault, C. P. Gros, J.-M. Barbe, R. Guillard, *IEEE Sens. J.* **2005**, *5*, 1–5; b) S. Clavaguera, P. Montméat, F. Parret, E. Pasquinet, J.-P. Lère-Porte, L. Hairault, *Talanta* **2010**, *82*, 1397–1402.

- [4] L. C. Shriver-Lake, B. L. Donner, F. S. Ligler, *Environ. Sci. Technol.* **1997**, *31*, 837–841.
- [5] For recent examples, see: a) G. Yang, C. Di, G. Zhang, J. Zhang, J. Xiang, D. Zhang, D. Zhu, *Adv. Funct. Mater.* **2013**, *23*, 1671–1676; b) N. Venkatarajah, S. Kumar, S. Patil, *Chem. Eur. J.* **2012**, *18*, 14745–14751; c) Y. Wang, A. La, Y. Ding, Y. Liu, Y. Lei, *Adv. Funct. Mater.* **2012**, *22*, 3547–3555; d) A. I. Costa, J. V. Prata, *Sens. Actuators B* **2012**, *161*, 251–260; e) C. Zhang, Y. Che, Z. Zhang, X. Yang, L. Zang, *Chem. Commun.* **2011**, *47*, 2336–2338; f) G. Tang, S. S. Y. Chen, P. E. Shaw, K. Hegedus, X. Wang, P. L. Burn, P. Meredith, *Polym. Chem.* **2011**, *2*, 2360–2368.
- [6] a) T. F. Jenkins, D. C. Leggett, P. H. Miyares, M. E. Walsh, T. A. Ranney, J. H. Cragin, V. George, *Talanta* **2001**, *54*, 501–513; b) A. Torres, I. Padilla, S. Huang, *Proc. SPIE-Int. Soc. Opt. Eng.* **2007**, 6553, 65531Q-1–165531Q-12; c) J. Patterson, *State-of-the-Art: Military Explosives and Propellants Production Industry, Vol 1*, American Defense Preparedness Association, Washington, **1976**.
- [7] P. A. J. Pella, *Chem. Thermodyn.* **1977**, *9*, 301–305.
- [8] a) K. J. Albert, D. R. Walt, *Anal. Chem.* **2000**, *72*, 1947–1955; b) R. Deans, A. Rose, K. M. Bardon, L. F. Hancock, T. M. Swager, Patent WO2008/073173 A2, **2008**; c) C. Cumming, M. Fisher, J. Sikes in *Electronic Noses & Sensors for the Detection of Explosives* (Eds: J. W. Gardner, J. Yinon), Kluwer Academic Publishers, London, **2004**, pp. 53–70.
- [9] a) S. W. Thomas III, T. M. Swager in *Aspects of Explosives Detection* (Eds.: M. Marshal, J. Oxley), Elsevier, Amsterdam, **2009**, pp. 203–221; b) D. McQuade, A. Pullen, T. Swager, *Chem. Rev.* **2000**, *100*, 2537–2574; c) S. Thomas, G. Joly, T. Swager, *Chem. Rev.* **2007**, *107*, 1339–1386; d) J. Yang, T. Swager, *J. Am. Chem. Soc.* **1998**, *120*, 5321–5322; e) J. Yang, T. Swager, *J. Am. Chem. Soc.* **1998**, *120*, 11864–11873; f) V. Williams, T. Swager, *Macromolecules* **2000**, *33*, 4069–4073; g) K. K. Kartha, S. S. Babi, S. Srinivasan, A. Ajayaghosh, *J. Am. Chem. Soc.* **2012**, *134*, 4834–4841; h) C.-P. Chang, C.-Y. Chao, J. H. Huang, A.-K. Li, C.-S. Hsu, M.-S. Lin, B. R. Hsieh, A.-C. Su, *Synth. Met.* **2004**, *144*, 297–301; i) A. Rose, Z. Zhu, C. Madigan, T. Swager, V. Bulovic, *Nature* **2005**, *434*, 876–879; j) Y. Liu, Y. Mills, J. Boncella, K. Schanze, *Langmuir* **2001**, *17*, 7452–7455; k) J. Cho, R. Anandakathir, A. Kumar, J. Kumar, P. U. Kurup, *Sens. Actuators B* **2011**, *160*, 1237–1243.
- [10] a) Y. Long, H. Chen, Y. Yang, H. Wang, Y. Yang, N. Li, K. Li, J. Pei, F. Liu, *Macromolecules* **2009**, *42*, 6501–6509; b) Y. Wang, N. B. McKeown, K. J. Msayib, G. A. Turnbull, I. D. W. Samuel, *Sensors* **2011**, *11*, 2478–2487.
- [11] a) S. Clavaguera, O. Dautel, L. Hairault, C. Méthivier, P. Montméat, E. Pasquinet, C. M. Pradier, F. Serein-Spirau, S. Wakim, F. Veignal, J. Moreau, J.-P. Lère-Porte, *J. Polym. Sci. Part A* **2009**, *47*, 4141–4149; b) S. Clavaguera, *Ph. D. Thesis*, University of Montpellier II, France **2007**.
- [12] a) M. Bouhadid, T. Caron, F. Veignal, E. Pasquinet, A. Ratsimihety, F. Ganachaud, P. Montméat, *Talanta* **2012**, *100*, 254–261; b) T. Caron, M. Guillemot, P. Montméat, F. Veignal, F. Perraut, P. Prené, F. Serein-Spirau, *Talanta* **2010**, *81*, 543–548; c) T. Caron, S. Clavaguera, M. Huron, E. Pasquinet, P. Montméat, L. Hairault, P. Prené, T. Flahaut, E. Schultz, F. Perraut, F. Serein-Spirau, *Mech. Chem. Eng. Trans.* **2010**, *23*, 25–29.
- [13] a) L. Wang, Y. Zhou, J. Yan, J. Wang, J. Pei, Y. Cao, *Langmuir* **2009**, *25*, 1306–1310; b) Y.-J. Shu, Y. Liu, Y. Xiong, X.-Y. Liu, Y.-J. Luo, X.-L. Hu, F.-C. Zhong, Y. Zhang, *New Trends Res. Eng. Mater.* **2010**, 39–49.
- [14] 2,4-DNT could not be used in this investigation due to low vapor pressure; therefore, toluene was chosen because of similarity in terms of aromatic character and molecule size.
- [15] S. Brunauer, L. S. Deming, W. E. Deming, E. Teller, *J. Appl. Ceram. Soc.* **1940**, *62*, 1723–1732.
- [16] J. R. Holst, A. Trewin, A. I. Cooper, *Nat. Chem.* **2010**, *11*, 915–920.
- [17] H. Li, D. Powell, R. Hayashi, R. West, *Macromolecules* **1998**, *31*, 52–58.
- [18] A. Mishra, R. Behera, P. Behera, B. Mishra, G. Behera, *Chem. Rev.* **2000**, *100*, 1973–2011.
- [19] B. Valeur, *Molecular Fluorescence*, Wiley-VCH, Weinheim **2002**.
- [20] a) S. Zahn, T. Swager, *Angew. Chem.* **2002**, *114*, 4399–4404; *Angew. Chem. Int. Ed.* **2002**, *41*, 4225–4230; b) M. Guo, O. Varnavski, A. Narayanan, O. Mongin, J.-P. Majoral, M. Blanchard-Desce, T. Goodson III, *J. Phys. Chem.* **2009**, *113*, 4763–4771; c) R. Lunt, J. Benziger, S. Forrest, *Adv. Mater.* **2009**, *21*, 1–4.
- [21] Q. Zhou, T. M. Swager, *J. Am. Chem. Soc.* **1995**, *117*, 12593–12602.
- [22] H. S. Carslaw, J. C. Jaeger in *Conduction of Heat in Solids*, Clarendon, Oxford, **1959**.
- [23] W. J. Bowyer, W. Y. Xu, J. N. Demas, *Anal. Chem.* **2004**, *76*, 4374–4378.
- [24] A. Montali, P. Smith, C. Weder, *J. Mater. Sci. Mater. Electron.* **2000**, *11*, 117–122.
- [25] E. Schultz, R. Galland, D. Du Bouëtiez, T. Flahaut, A. Planat-Chrétien, F. Lesbire, A. Hoang, H. Volland, F. Perraut, *Biosens. Bioelectron.* **2008**, *23*, 987–994.
- [26] V. Rouessac, A. van der Lee, F. Bosc, J. Durand, A. Ayral, *Microporous Mesoporous Mater.* **2008**, *111*, 417–428.
- [27] T. Mérian, D. Debarnot, V. Rouessac, F. Poncin-Epaillard, *Talanta* **2010**, *81*, 602–608.
- [28] L. Palatinus, C. Chapuis, *J. Appl. Crystallogr.* **2007**, *40*, 786–790.
- [29] P. W. Betteridge, J. R. Carruthers, R. I. Cooper, K. Prout, D. J. Watkin, *J. Appl. Crystallogr.* **2003**, *36*, 1487.
- [30] L. Schouffeten, P. Denjean, G. Joliff-Botrel, C. Bernard, D. Pansu, R. B. Pansu, *Photochem. Photobiol.* **1999**, *70*, 701–709.
- [31] J.-A. Spitz, R. Yasukuni, N. Sandeau, M. Takano, J.-J. Vachon, R. Méallet-Renault, R. B. Pansu, *J. Microsc.* **2008**, *229*, 104–114.

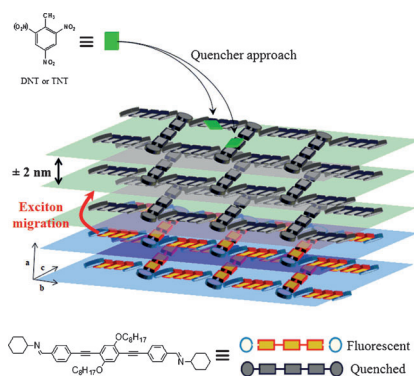
Received: March 12, 2014

Revised: July 2, 2014

Published online on ■■■■■, 0000

## FULL PAPER

**Explosive sensing:** A structural mechanism that takes into account both the special conformation of oligophenylethyne molecules at a thin-film surface and antenna effects enabled by exciton migration is presented (see figure). This mechanism explains why these crystallized fluorescent films exhibit excellent sensing properties toward nitroaromatic vapors despite the fact that they are nonporous.



## Thin Films

T. Caron, E. Pasquinet, A. van der Lee,  
R. B. Pansu, V. Rouessac, S. Clavaguera,  
M. Bouhadid, F. Serein-Spirau,  
J.-P. Lère-Porte, P. Montméat\*

Efficient Sensing of Explosives by  
Using Fluorescent Nonporous Films of  
Oligophenylethyne Derivatives  
Thanks to Optimal Structure  
Orientation and Exciton Migration

